










Article

A Micro-Tomographic Insight into the Coating Systems of Historical Bowed String Instruments

Giacomo Fiocco ^{1,2}, Tommaso Rovetta ¹, Claudia Invernizzi ^{1,3}, Michela Albano ¹, Marco Malagodi ^{1,4}, Maurizio Licchelli ¹, Alessandro Re ⁵, Alessandro Lo Giudice ⁵, Gabriele N. Lanzafame ⁶, Franco Zanini ⁶, Magdalena Iwanicka ⁷, Piotr Targowski ⁸ and Monica Gulmini ^{2,*}

- ¹ Laboratorio Arvedi di Diagnostica Non-Invasiva, CISRiC, Università degli Studi di Pavia, Via Bell'Aspa 3, 26100 Cremona, Italy; giacomo.fiocco@unipv.it (G.F.); tommaso.rovetta@unipv.it (T.R.); claudia.invernizzi@unipv.it (C.I.); michela.albano@unipv.it (M.A.); marco.malagodi@unipv.it (M.M.); maurizio.licchelli@unipv.it (M.L.)
- ² Dipartimento di Chimica, Università di Torino, Via Pietro Giuria 5, 10125 Torino, Italy
- ³ Dipartimento di Scienze Matematiche, Fisiche e Informatiche, Università degli Studi di Parma, Parco Area delle Scienze 7/A, 43124 Parma, Italy
- ⁴ Dipartimento di Musicologia e Beni Culturali, Università degli Studi di Pavia, Corso Garibaldi 178, 26100 Cremona, Italy
- ⁵ Dipartimento di Fisica, Università di Torino and INFN, Sezione di Torino, Via Pietro Giuria 1, 10125 Torino, Italy; alessandro.re@unito.it (A.R.); alessandro.logiudice@unito.it (A.L.G.)
- ⁶ Elettra-Sincrotrone Trieste S.C.p.A., S.S. 14 km 163.5, Basovizza, 34194 Trieste, Italy; gabriele.lanzafame@gmail.com (G.N.L.); franco.zanini@elettra.eu (F.Z.)
- ⁷ Institute of Art Conservation Science, Department of Fine Arts, Nicolaus Copernicus University, Sienkiewicza 30/32, 87-100 Toruń, Poland; magiwani@gmail.com
- ⁸ Institute of Physics, Department of Physics, Astronomy and Informatics, Nicolaus Copernicus University, Grudziądzka 5, 87-100 Toruń, Poland; ptarg@fizyka.umk.pl
- * Correspondence: monica.gulmini@unito.it; Tel.: +39-011-670-5265

Received: 21 December 2018; Accepted: 28 January 2019; Published: 29 January 2019



Abstract: Musical instruments are tools for playing music, but for some of them—made by the most important historical violin makers—the myths hide the physical artwork. Ancient violin-making Masters developed peculiar construction methods and defined aesthetic canons that are still recognizable in their musical instruments. Recently, the focus of scientific investigations has been set on the characterization of materials and methods used by the ancient violin makers by means of several scientific approaches. In this work, the merits of synchrotron radiation micro-computed tomography and optical coherence tomography (OCT) for the investigation of complex coatings systems on historical bowed string musical instruments are discussed. Five large fragments removed during past restorations from instruments produced by Jacobus Stainer, Gasparo da Salò, Giovanni Paolo Maggini, and Lorenzo Guadagnini have been considered for a non-invasive insight by tomographic techniques and the results are discussed considering previous micro-invasive investigations. The tomographic approach allows to highlight the micro-morphology of the coating systems and offers preliminary information on the methods that were employed by the ancient Masters to treat the wood and finish the musical instrument.

Keywords: varnish; musical instruments; tomography; synchrotron radiation micro-computed tomography; micro-CT; optical coherence tomography; OCT

1. Introduction

Some historical bowed string musical instruments produced in Brescia and Cremona (Italy) from the 16th to the 18th centuries have acoustic features and aesthetic appeal that are still considered inimitable. During the whole history of violin making, from the past till nowadays, technical skills of the Masters and the materials they used in the grounding and varnishing treatments after the assemblage of the instrument play a decisive role in determining the exceptional acoustic performances of the instruments [1]. The finishing processes were kept secret by the violin makers and the traditional methods were passed down from master craftsmen to apprentices. Nevertheless, this knowledge—matured over two centuries of violin making—has been lost during the second part of the 18th century, when the most prominent historic families and their workshops disappeared [2]. Nowadays, methods and materials of past violin making workshops represent a charming secret to be revealed through scientific investigations, in order to enable modern violin makers to reproduce the techniques, and possibly, the aesthetic excellence of the instruments produced by the old Masters, therefore supporting the stakeholders in conservation and restoration procedures [3].

During the last decade, scientists have proposed analytical protocols and procedures dedicated to the identification and characterization of the materials. The musical instruments were tested both through the most common non-invasive spectroscopic techniques [4–9], such as X-ray fluorescence (XRF), Raman spectroscopy, and Fourier transform infrared spectroscopy (FTIR) in ATR and reflection mode, and by micro-invasive analyses, such as micro-FTIR and scanning electron microscopy coupled with energy dispersive x-ray analysis (SEM-EDX) [10–14]. These works allowed scientists to highlight the diversity of the materials used by the ancient violin makers. The presence of a multi-layered coating system frequently composed of a very thin proteinaceous preparation, applied directly on the wooden substrate, and an oil-resinous varnish has been detected in several musical instruments manufactured both in Brescia and Cremona. Moreover, some inorganic materials, such as sulfates, carbonates, and silicates [4,8,12,15–17], as well as dispersed colorants [6,13,18–22], were identified. The characterization of this wide variety of organic and inorganic materials—combined together in order to seal the wood porosity, protect the instrument from moisture and biological agents, and enhance its aesthetic appearance—represents the most challenging task in the investigation of the finishing layers in historic musical instruments.

Specific analytical issues emerge when the sampling is not feasible because of the need to preserve the value and the integrity of the precious artefacts. Under this scenario, the multi-analytical approach allows scientists to improve the interpretation of the results obtained by a single non-invasive technique, in order to significantly enhance the power of the interpretation of the stratigraphic sequence without sampling. Among the most promising non-invasive techniques, micro-tomographic ones certainly play a prominent role [23], but their application to the investigation of coating systems in historical bowed string instruments is presently rare [24–27].

Basically, tomographic investigations are powerful tools that allow researchers to catch a non-invasive insight into the morphology of a large number of materials, albeit without information on chemical composition. X-ray computed tomography (CT) and optical coherence tomography (OCT) are probably the most common techniques used for this purpose. Computed tomography employs X-rays for obtaining morphological and physical information on the inner structure of an object and is frequently applied for the full-volume inspection of samples from the cultural heritage [23,28–30]. The high-flux polychromatic beam used in synchrotron radiation micro-computed tomography (SR-micro-CT) let to measurements at high spatial resolution. In 2012, this technique was applied for the first time to bowed string musical instruments at the Elettra synchrotron laboratory (Trieste, Italy) with the aim of gathering morphological information on the violin as a whole, by using spatial resolutions ranging between 9 and 50 μm [31,32]. After some years, a micro-tomographic investigation—with a spatial resolution of 1 μm —was conducted in the same facility in order to set up a procedure properly focused on the study of the coatings of these peculiar objects [33]. These examinations were complemented by optical coherence tomography imaging, an optical broad-band interferometric

non-invasive technique. Optical coherence tomography is well established as a diagnostic method in ophthalmology and has been successfully used for examination of objects of art since 2004 [34,35]. In the cultural heritage field, OCT is generally used to investigate the object's stratigraphy in terms of layers' thickness measurements, providing information about the presence of particles as well as cracks, delaminations and other optical destruction phenomena [36,37]. The application of OCT for the inspection of coating systems on historical violins was previously addressed by Latour et al. [25].

In this work, the merits of tomographic techniques in the investigation of finishing layers on musical instrument are further considered. Five fragments, selected from a large collection, have been scanned by means of the two tomographic approaches mentioned above: SR-micro-CT and OCT. The fragments were obtained during past restorations, in which damaged parts of the original instrument have been replaced. The restorations were performed during the first half of the 20th century by the famous Italian violin makers Gaetano and Pietro Sgarabotto, who kept the original fragments as models for the varnish of their new instruments. The set of the historical fragments, named "Collezione Sgarabotto", was subsequently exposed in the violin making school of Cremona for about thirty years [38]. The selected fragments previously underwent an in-depth analytical campaign focused on the finishing layers, and the results concerning the chemical composition of the materials employed—as well as the hypothetical sequence of the finishing layers—are reported in [11,12]. Data from these publications have been carefully considered in this work in order to compare the chemical and physical data with the morphological view obtained by tomography. In particular, the two tomographic techniques are evaluated here by testing—on historical samples—their ability to highlight the presence of many overlying finishing layers and to measure their thickness. Particular attention is set on the interface between the wood and the coating system, as the morphology is detected here without any possible disturbance arising from sampling. Moreover, the work also aims at checking the effectiveness of the techniques in: (i) detecting the presence of dispersed particles, (ii) giving an overview on their concentration in each layer, and (iii) highlighting some of their morphological features, such as mean grain-size and tendency to form aggregates.

2. Experimental

2.1. Synchrotron Radiation Micro-Computed Tomography

The three-dimensional micromorphology study of the fragments was performed by high-resolution SR-micro-CT in phase-contrast mode [39] at the SYRMEP beamline of the Elettra synchrotron laboratory (Trieste, Italy) (Figure 1a). A polychromatic X-ray beam delivered by a bending magnet source illuminated the sample in transmission geometry. Regarding the white beam, filters (1.5 mm Si + 1 mm Al) were used to suppress the contribution of low energies in the beam spectrum. With this configuration the average beam energy resulted to be about 28 keV. The sample-to-detector distance was set at 150 mm. For each experiment, 1800 projections were recorded rotating the sample continuously over an angle of rotation of 180 degrees, with an exposure time/projection of 0.25 s. The detector used was a Hamamatsu C11440-22C air-cooled, 16 bit, sCMOS camera (Hamamatsu Photonics, Hamamatsu, Japan) with a 2048×2048 pixels chip. Measurements were carried out with an effective pixel size of the detector set at $(1 \times 1) \mu\text{m}^2$; measurements were carried out with an effective pixel size of the detector set at $(1 \times 1) \mu\text{m}^2$ yielding a maximum field of view of about $(2.4 \times 2.4) \text{mm}^2$.

The reconstruction of the 2D tomographic slices was done with the SYRMEP Tomo Project (STP) house software suite [40]. Different combinations of the filters available in the STP software (v.1.2.5) were applied to the datasets, in order to reduce ring artefacts caused by detector inhomogeneity [41]. The consistency of the morphological analysis was improved applying a single-distance phase-retrieval algorithm [42] based on the Transport of Intensity Equation (TIE) to the sample projections. This can be done by computing the complex refractive index of the samples $n = 1 - \delta + i\beta$, (where δ is the real and β the imaginary part, related to phase and absorption distribution of the sample, respectively). A constant ratio $\gamma = \delta/\beta = 151$ was determined to be the best suitable for the investigated samples.

Phase-retrieval, in combination with the Filtered Back-Projection algorithm [43], allowed to obtain the 3D distribution of the complex refraction index of the imaged samples in order to reduce the edge-enhancement effect at sample borders, preserving the morphology of the smallest features. The stack of slices was imported in VGStudio Max 2.2 from Volume Graphics: it was then used both for the 3D rendering and segmentation (manual thresholding) of the volumes (Figure 2). The 3D virtual reconstructions were elaborated using Photoshop CS6 starting from the tomographic volumes.

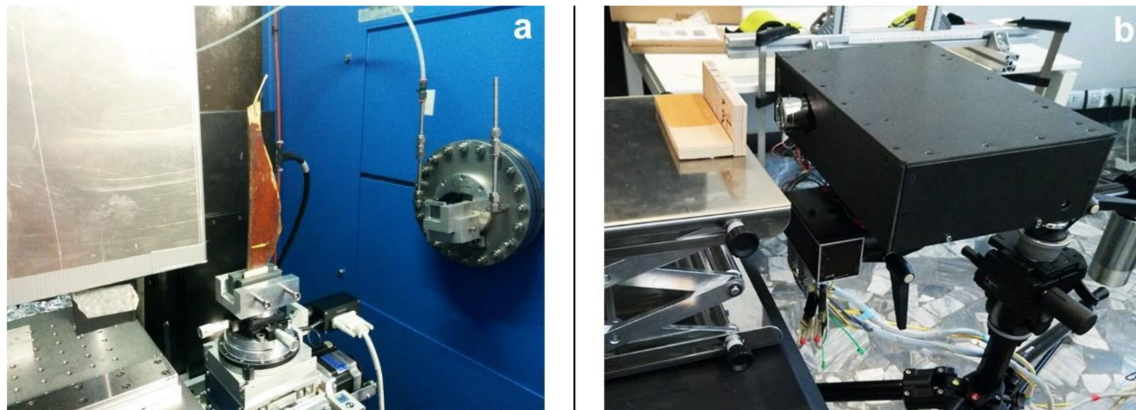


Figure 1. Tomographic setups: (a) high-resolution SR-micro-CT in phase-contrast mode at the SYRMEP beamline of the Elettra Synchrotron laboratory (Trieste, Italy); (b) prototype high-resolution portable Spectral domain optical coherence tomography (SdOCT) instrument built at N. Copernicus University for FP 7 CHARISMA project.

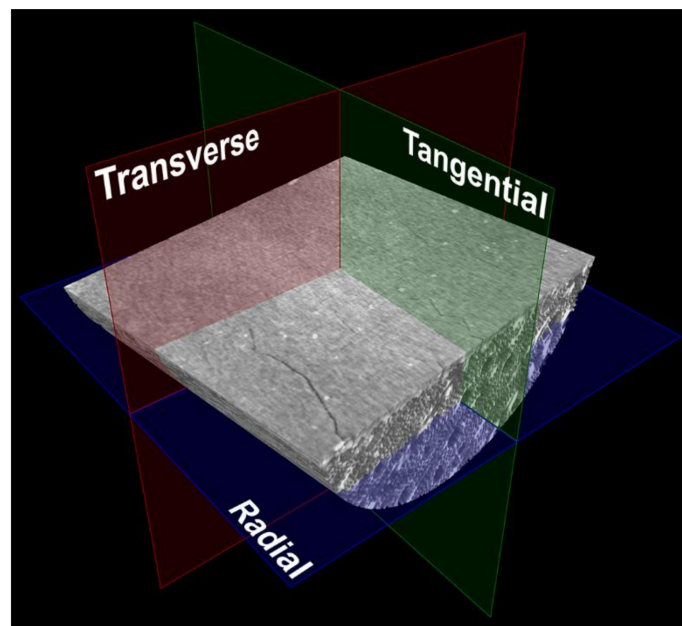


Figure 2. Planes considered for the virtual slicing of SR-micro-CT volume renderings (fragment F01 is shown here as an example). These planes produce 2D images of radial, tangential, and transverse sections of the wood.

2.2. Optical Coherence Tomography

The examination of the fragments was performed in the Arvedi Laboratory of Non-Invasive Diagnostics hosted in the Museo del Violino (Cremona, Italy), within the MOLAB Transnational Access-EU H2020 Project IPERION CH. The study was carried out with a laboratory-built high-resolution portable Spectral domain optical coherence tomography (SdOCT) (Figure 1b) [44]. It comprises a broad-band light source made up of coupled super-luminescent LEDs emitting in a

band of 750–930 nm. The intensity of radiation at the object never exceeded 800 μW , and due to fast scanning, it was focused at any given spot on the object for only 45 μs . The lateral imaging resolution was about 15 μm , whereas the axial one was 3 μm in air, with an axial imaging range of ca 2.0 mm. It is important to point out that the distances along the probing beam, that is to say the depths, represent optical distances in OCT, and this must be taken into account when true axial distances within the object structure are measured. For this reason, all of the axial distances should be corrected for the refractive index of the medium as it is in the case of all images presented herein. Thus, the axial resolution in the transparent varnish layer ($n_R = 1.5$) may be estimated to be ca 2 μm . Therefore, in order to identify a structure as a layer (to see its both interfaces separately) it needs to be a minimum of 5 μm thick. The distance to the object from the most protruding element of the device was 43 mm. Data for OCT images were collected from adjacent locations by scanning the probing beam along a straight line (i) of 10 mm length for fragments F1, F16, and F21 and (ii) of 8 mm length for fragments F13 and F20, over 135 ms in both cases. The resultant tomograms—or B-scans—are presented in false-color scale with colors assigned automatically by the software. Black areas in the tomograms are those for which no scattering of the probing radiation is detected, either due to the intrinsic properties of the material (as for air, for instance) or because these areas are not reached by the radiation. Areas with detectable—albeit low—scattering properties were colored from blue to green. Centers of medium-to-high scattering properties were colored from yellow to red, respectively. The tomograms were vertically stretched about eight-fold for a better readability of the coating system. It must be noted that data for this contribution were accumulated by collection of a series of adjacent, parallel B-scans and for presentation the most representative ones were chosen arbitrarily, regardless of their actual direction in relation to the original musical instrument. Specifically, fragments F1, F16, and F21 were scanned over area of $(10 \times 10) \text{ mm}^2$ and fragment F20 over $(8 \times 8) \text{ mm}^2$ —as series of 100 B-scans—in 13.5 s each and the fragment F13 was scanned over $(8 \times 4) \text{ mm}^2$ in 50 scans in overall time of 6.75 s [45].

3. Results and Discussion

Results for each sample are reported and discussed in following paragraphs within the frame of the morphological and chemical characterization reported in previous papers [11,12]. Moreover, previous and present results are outlined in Table 1, which gives a schematic comparison of the layers according to the different investigative approaches.

3.1. F01-Jacobus Stainer

The analyses reported in Fiocco et al. [12] suggested for fragment F01 the presence of a proteinaceous-based preparation on the maple substrate—with a homogeneous thickness of about 15 μm —and an upper oil-based varnish layer 30- μm thick. In addition, some carbonate particles and iron-based pigments were found respectively in the preparation layer and in the upper oil-based varnish [12].

Observing the stratigraphic sequence through SR-micro-CT 2D slices (Figure 3a–e), it is possible to confirm the stratigraphy of the coating system: upon the maple wood substrate (indicated as A in Figure 3a) a preparation layer (indicated as B in the same picture) and an upper varnish layer (C) were identified. In addition, an external layer (D) 10- μm thick—which appears brighter than the underlying one—was also visible. Furthermore, the SR-micro-CT investigation allowed to confirm at least three different particles included in the superimposed layers. The main morphological features of the particles were evident in radial slices, reported in Figure 3b–e. Some of them were fine (diameters of about 5 μm) (Figure 3a,c; P1), identified at the interface between the wood and the preparation layer; some particles with a diameter of 5–10 μm were spread homogeneously within the varnish layer (Figure 3a,d; P2); moreover, thinner ones which were not detected in the previous analyses, have been identified in the external layer (Figure 3a,e; P3). The 3D virtual reconstruction in Figure 3f

clearly shows the dispersion of the different inclusions, represented with false colors according to their position in the coating system.

The OCT examination (Figure 3g) discriminates two layers applied over the wood (A): the bottom layer (B in Figure 3f) is about 12- μm thick, much thinner than the upper one (C) whose thickness varies from 26 to 33 μm . Some dispersed particles are clearly observed both in the preparation layer (Figure 3g; P1) and in the varnish where lots of them sedimented to the bottom of this coat (Figure 3g; P2). It was not possible to identify the third layer (D) highlighted by the SR-micro-CT 3D model (Figure 3f), probably due to the similar optical properties of the (C) and (D) layers, which resulted in imaging them as one stratum. This hypothesis could also explain why the thickness estimated by OCT results is slightly greater than that estimated by SR-micro-CT.

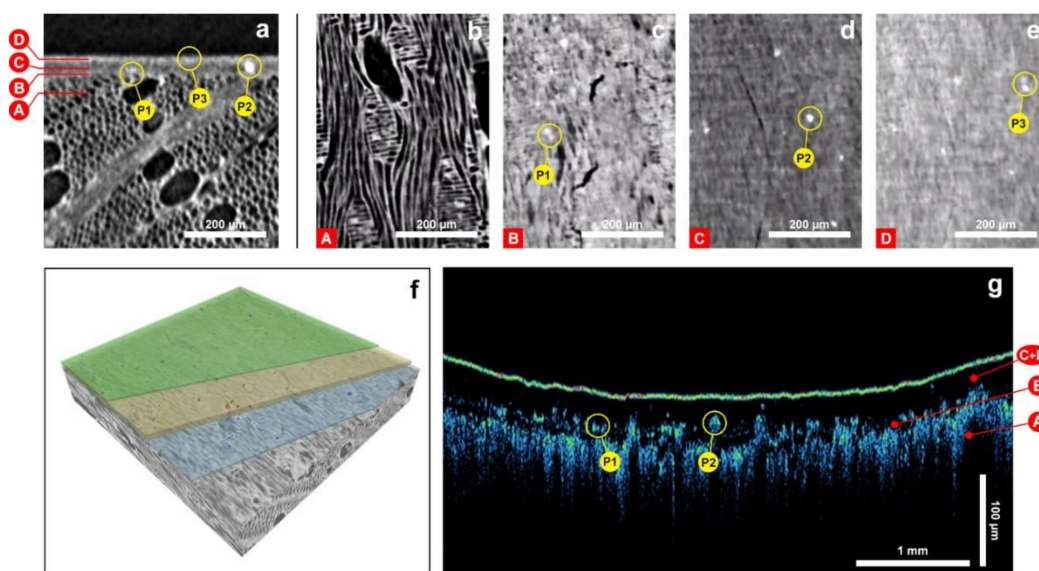


Figure 3. Fragment F01, Jacobus Stainer. (a) Transverse slice from the SR-micro-CT volume with the identified layers; different layers are highlighted in capital letters and different particles are indicated as P1, P2, and P3. (b–e) Radial slices from the SR-micro-CT volume showing the finishing layers discussed in the text and reporting the particles P1, P2, and P3 indicated in (a) and identified at different depth. (f) Virtual reconstruction based on SR-micro-CT volume. The preparation layer (B in Figure 3a) is colored in blue with dark blue particles; the varnish layer C is shown in yellow with particles colored in red and the outermost layer D is green with violet particles. (g) The OCT tomogram presented in false-color scale (see Section 2.2 for details). The wood substrate A, the preparation layer B, and the varnish layer C + D are shown. Particles embedded in the preparation layer and in the varnish are indicated as P1 and P2, respectively.

Table 1. List of the selected historical musical instruments fragments with a schematic comparison of the finishing layers according to previous data [11,12] and to the present results from SR-micro-CT and OCT scans. Capital letters indicate each layer are the same as those in Figures 3–7. Horizontal lines guide the eye and separate the detected layers.

Fragment	Layer	Microscopic Examination & Chemical Analyses [11,12]	SR-Micro-CT	OCT
J. Stainer F01-Cello	D	Not detected	10- μ m thick layer with particles	26–33 μ m thick layer with particles
	C	30- μ m thick oil-based varnish containing Fe-based pigments	20- μ m thick layer with particles	
	B	15- μ m thick proteinaceous binder containing carbonate-based particles	10–15 μ m thick layer with particles	12- μ m thick layer
	A	Maple wood	Maple wood	Wood substrate (not recognized)
Gasparo da Salò F13-Cello	D	Layer with organic black particles 10- μ m thick layer with inorganic particles (5 μ m)	10–15 μ m thick layer with particles	15- μ m thick layer composed by two thin layers with particles
	C	5- μ m thick layer with inorganic particles	10–15 μ m thick layer with particles	
	B	10- μ m thick layer with Fe-based pigments and gypsum grains (5–10 μ m)		
	A	Proteinaceous binder with black particles and Fe-based particles Maple wood	Not detected Maple wood	Thin layer detected Wood substrate (not recognized)
Gasparo da Salò F16-Cello	C	5- μ m thick layer embedding organic black particles	Layer with two types of particles identified through grayscale variations Maple wood	10–19 μ m thick layer with particles
	B	20- μ m thick layer with Fe-based (2–3 μ m) and Pb-based (15–20 μ m) particles		23–26 μ m thick layer with particles
	A	Maple wood		Wood substrate (not recognized)
G.P. Maggini F20-Double Bass	C	30- μ m thick varnish layer with Fe-based particles (2–3 μ m)	30- μ m thick layer with particles (2–3 μ m)	19–36 μ m thick layer
	B	Not detected	Not detected	9–12 μ m thick layer
	A	Maple wood	Maple wood	Wood substrate (not recognized)
L. Guadagnini F21-Double Bass	C	50- μ m thick layer	Layer with cracks, air bubbles and particles	30–50 μ m thick layer with cracks and particles
	B	10 μ m thick layer with Fe-based and gypsum particles	Layer with particles	12–15 μ m thick layer
	A	Spruce wood	Spruce wood	Wood substrate (not recognized)

3.2. F13-Gasparo da Salò

By inspecting under an optical microscope with visible and UV illumination a sample detached from the fragment F13, Fichera et al. [11] recognized at least five layers and a large number of organic and inorganic particles dispersed in them. A thin preparation layer was applied directly over the maple wood as sealer, and several organic thin black particles and some iron-based pigment particles were identified in this coat. An upper layer—some 10- μm thick—contained two different types of particles—identified as iron-based pigments—and few larger (5–10 μm) grains of gypsum. A further layer—thinner than 5 μm —was also highlighted. The upper varnish layer showed a uniform thickness of about 10 μm without evidence of embedded particles. Finally, the most external coat was found to contain a fine dispersion of black particles.

In contrast to the very complex system previously reported [11], the micro-tomographic investigation has enabled the detection of two layers (Figure 4). Observing the SR-micro-CT 2D transverse and tangential slices (Figure 4a,b), no evidences of a thin preparation layer have been found. This layer has been instead detected by OCT (see below) and is indicated as B in Figure 4. The two layers detected by SR-micro-CT (C and D in Figure 4a) show an overall thickness of about 20–25 μm ; they have been distinguished on the basis of two distinct types of inorganic particles—indicated as P1 and P2 in Figure 4—dispersed at a different depth. The particles appear bright in the images and their distribution in the coating system is clearly displayed by radial slicing (Figure 4c–e).

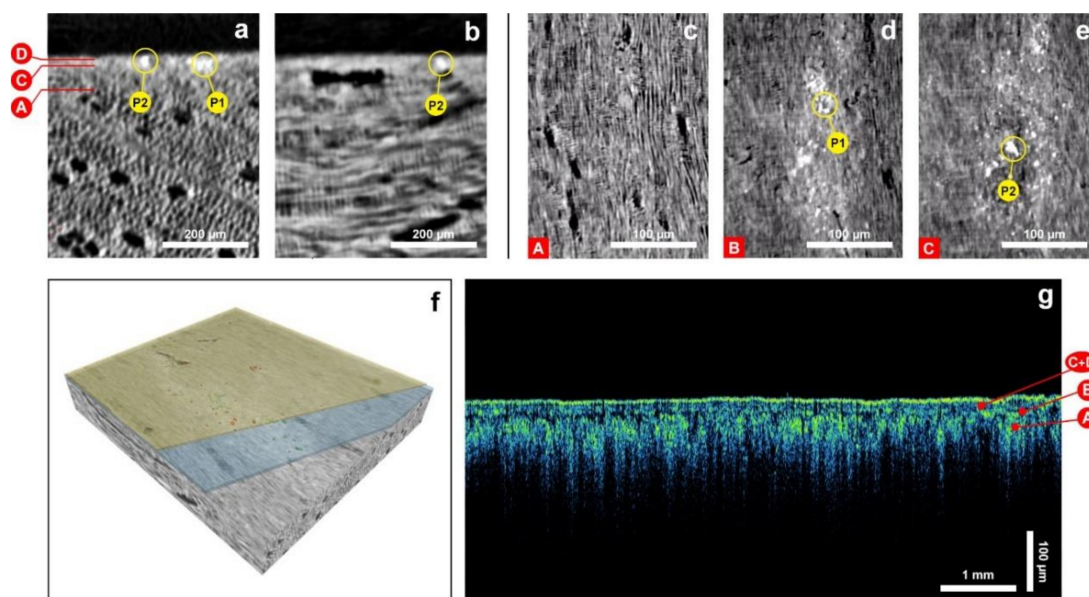


Figure 4. Fragment F13, Gasparo da Salò. (a,b) Transverse and tangential slices from the SR-micro-CT volume showing the levels for radial slices reported in (c–e) and the different kinds of particles embedded in the finishing layers. (c–e) Radial slices from the SR-micro-CT volume showing the finishing layers discussed in the text. (f) Virtual reconstruction based on SR-micro-CT volume. Layer C (as in Figure 4a) is colored in blue with green particles and layer D is shown in yellow with red particles. (g) OCT tomogram presented in false-color scale (see Section 2.2 for details). On the wood substrate A, a preparation layer B appears as the dark, non-scattering structure; the varnish shows two barely visible layers (C + D) with fine scattering particles.

The overall picture obtained by the SR-micro-CT scans is reported in the 3D virtual reconstruction of Figure 4f; the first layer detected on the wood has been colored in blue (and the particles P1 dispersed in it has been colored in green), whereas the varnish layer and the P2 particles in it have been colored yellow and red, respectively. Although the observation of the cross section under the optical microscope suggested a different mean size for the particles dispersed in different layers [11],

the general picture emerging from the SR-micro-CT scan does not support this picture, as no bimodal distribution is evident from Figure 4f.

Comparing the complex stratigraphy [11] with the more simple 3D virtual reconstruction (Figure 4f) it is possible to suggest a correspondence between the five layers highlighted by optical microscopy and the two layers detected by SR-micro-CT. Considering the thickness that have been evaluated for each layer—and the distribution of the detected particles—the first two layers on the wood (10–15 μm of overall thickness, according to previous investigations) may have been recognized as one in the SR-micro-CT images (Figure 4a, layer C; Figure 4f, blue layer), whereas the outer three layers (10–15 μm of thickness) could have virtually merged into one in the SR-micro-CT images (Figure 4a, layer D; Figure 4f, yellow layer).

In the images produced by OCT (Figure 4g), only some of the layers are evident. This result is reasonable if the instrument's axial resolution is taken into consideration, since the thickness of some layers is expected to be equal to or less than 5 μm . This is the case of the uppermost layer, estimated to be 5- μm thick by Fichera et al. [11]. In the OCT tomogram, two light-scattering layers—of an altogether thickness of 15 μm —were observed (Figure 4g; layers C + D). They lay on the top of a non-scattering thin layer—indicated as B in Figure 4g—which could be correlated to the thin preparation layer containing an organic dispersion previously identified [11]. The particles embedded in the varnish layers are too fine to be imaged as separate structures in the OCT image (below lateral resolution—15 μm). Nonetheless, their presence is confirmed by the high scattering of light detected in the layers.

3.3. F16-Gasparo da Salò

This second fragment by Gasparo da Salò has a simpler coating system compared to F13, with two layers superimposed on the treated wooden substrate: the first layer—attributed to the varnish—showed a thickness of about 20 μm while an upper thinner layer of some 5 μm was also detected. In addition, at least two different types of particles were identified in the varnish layer: some red fine particles of about 2–3 μm in diameter and some larger grey particles of about 15–20 μm . The red grains were identified as Fe-based pigments, probably red ochre, while the bigger ones are Pb-based grains. Furthermore, some gypsum-based particles were identified between the wood and the first layer as filler and some organic black particles were identified in the most external layer [11].

The observation of the SR-micro-CT 2D transverse and radial slices (Figure 5a,b) indicated the presence of a varnish layer (B) over the wooden substrate with cracks (Figure 5c; F1). Moreover, several bright-white particles (Figure 5; P1,2) were dispersed in layer B. Focusing on the greyscale and on the size of the particles, the smaller Pb-based particles (Figure 5a,c; P1) can be discriminated from the larger red ochre (Figure 5a,c; P2). The virtual 3D reconstruction in Figure 5e indicates a homogeneous distribution of the inorganic pigments in the varnish and highlight the evident bimodal distribution of the grain-size. No evidence of any further external coating [11] was found, probably due to the very reduced thickness of this layer and the very reduced differences in its composition with respect to the underlying varnish, or because of an inhomogeneous distribution of the layering, which might lack of the most external layer in some parts of the considered fragment.

On the other hand, the OCT has been able to discriminate both the two organic layers previously detected, as well as numerous particles dispersed therein (Figure 5f; P1–3). The thickness of the varnish layer B resulted to be between 23 and 26 μm , i.e., fairly consistent with the thickness previously detected by optical microscopy [11], while layer C resulted thicker (10–19 μm) by OCT if compared to the 5 μm recorded under the optical microscope. Nevertheless, a slight variation of the layer's thickness in different areas is expected for coatings laid by brush.

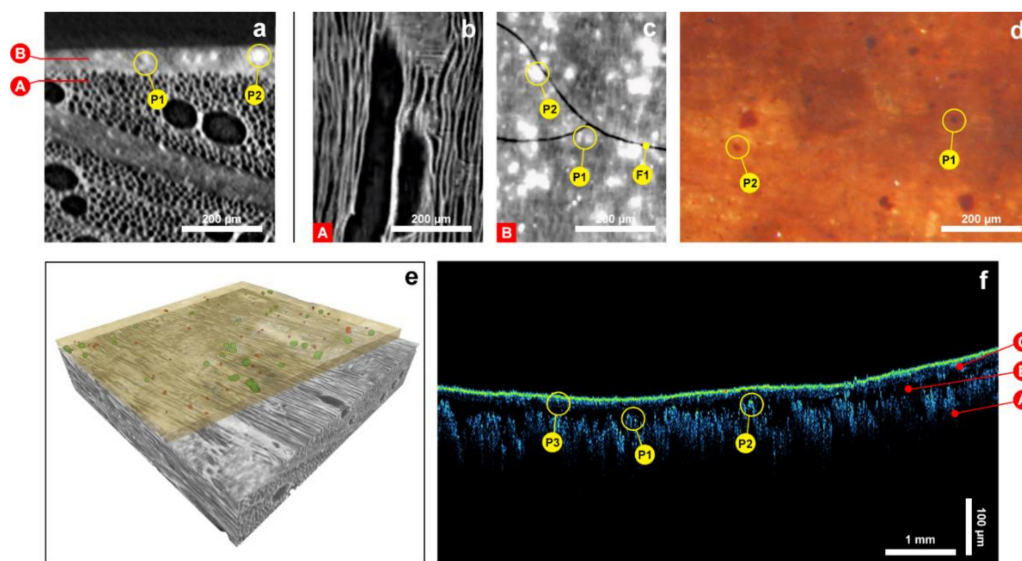


Figure 5. Fragment F16, Gasparo da Salò. (a) Transverse slice from the SR-micro-CT volume with the identified layers; different layers are highlighted in capital letters and different particles are indicated as P1 and P2. (b,c) Radial slices from the SR-micro-CT volume showing the finishing layers discussed in the text and reporting the particles P1 and P2 indicated in (a) and identified at different depth. Cracks are indicated as F1. (d) Stereomicroscopic image of the surface showing the different particles P1 and P2, embedded in the finishing layer. (e) Virtual reconstruction based on SR-micro-CT volume. The varnish layer (B in Figure 5a) is colored in yellow, whereas Pb-based particles and red-ochre particles embedded in the varnish are colored in red and green, respectively. (f) OCT tomogram presented in false-color scale (see Section 2.2 for details). The wood substrate A, the varnish layer B, and the external layer C are shown. Particles embedded in the varnish layer and in the external layer are indicated as P1, P2, and P3, respectively.

3.4. F20-Giovanni Paolo Maggini

The fragment detached from a cello attributed to Maggini has a double-layer coating system spread over the maple substrate. A thin preparation layer fills the wood pores and an external varnish layer (25–30 μm thick) completes the coating system. In addition, some rare red ochre particles (2–3 μm across) dispersed in the varnish are present [11].

The 2D slices obtained through SR-micro-CT (Figure 6a–e) allowed us to accurately observe the wood substrate (A), identifying a woodworm tunnel (diameter about 1 mm) that runs some microns under the finishing layers (Figure 6b,c). Unfortunately, no evidence of the upper preparation layer (B) have been found. Observing the slices, only one varnish layer is clearly visible (C), which has a thickness of about 30 μm , with some rare dispersed particles (Figure 6a,e; P1) attributable to the red ochre particles, as suggested by the previous chemical analysis [11]. The 3D volume rendering is very useful to highlight the distribution and the low concentration of the particles (Figure 6f).

This OCT technique validated the thickness of the layer (C), with a measure ranging from 19 to 36 μm , resulting fairly in accordance with the observations by optical microscopy on the cross section and by SR-micro-CT on the fragment. The technique was also able to detect the thin layer (9–12 μm thick) between the varnish and the wood, identified as the preparation layer (B): in fact, the presence of centers with moderate scattering properties (highlighted in Figure 6g), defines the boundary between the layers (B) and (C).

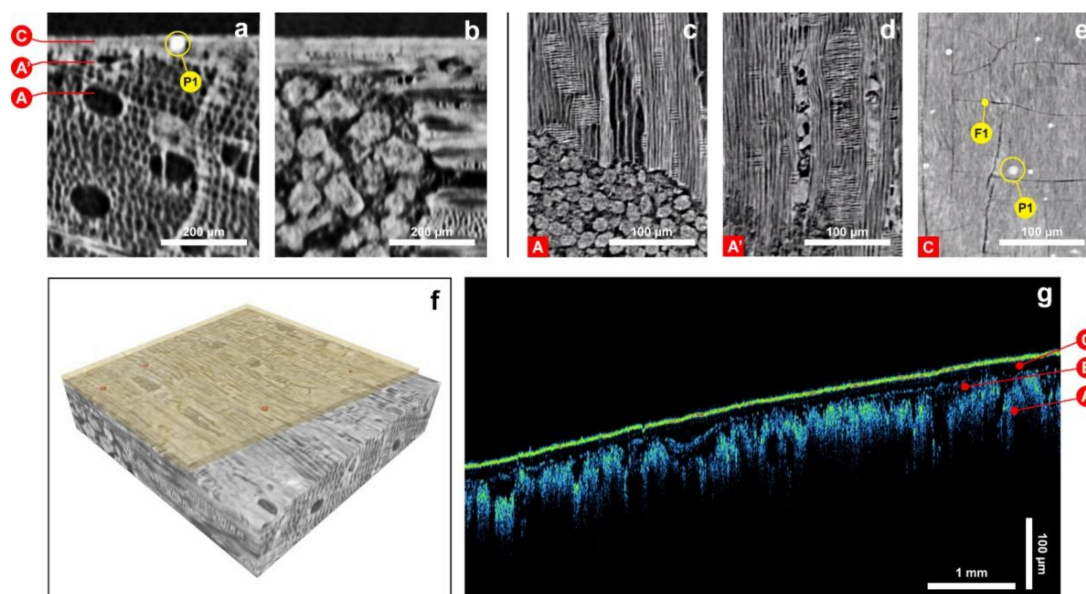


Figure 6. Fragment F20, Giovanni Paolo Maggini. (a,b) Transverse and tangential slices from the SR-micro-CT volume showing the particles P1 embedded in the finishing layers. Signs of previous infestation by woodworms are visible in (a). (c–e) Radial slices from the SR-micro-CT volume showing the finishing layers discussed in the text. Particles and cracks are indicated as P1 and F1, respectively. Signs of woodworms are visible in (c). (f) Virtual reconstruction based on SR-micro-CT volume. The varnish (layer C in Figure 6a) is colored in yellow and particles in red. (g) OCT tomogram presented in false-color scale (see Section 2.2 for details). The wood substrate A, the preparation layer B, and the varnish layer C are shown.

3.5. F21-Lorenzo Guadagnini

The stratigraphy of the coating system for the fragment attributed to Lorenzo Guadagnini was described in Fiocco 2017, and appeared composed of two overlying layers. In the sample that was considered for this previous investigation, the tracheids of the spruce wood appear deformed at the wood-to-varnish interface. The first layer—10- μm thick—was interpreted as a colored preparation and showed two different types of particles dispersed in it: some grains attributed to a red ochre pigment and some other particles identified as gypsum. In the upper varnish layer—about 50- μm thick—no particles were detected [12].

The 2D SR-micro-CT slices (Figure 7a–d) allowed us to draw a more in-depth interpretation of the stratigraphy: the upper tracheids of the wood substrate (indicated as A in Figure 7) near the first superimposed layer (indicated as B), are visible in the radial slices (Figure 7c) and appear as partially filled by this preparation layer. Furthermore, some fine bright particles (indicated as P1) have been detected at the interface with the wooden substrate (Figure 7a,c). The deformation of the tracheids is not confirmed here by the radial slicing of the tomographic volume. Therefore, the spoil of the original shape of the wood structure shall be more properly interpreted as a disturbance occurred on sampling instead of a previous treatment intentionally performed to seal the wood porosity. The observation of the upper thick varnish layer (C) confirms the thickness measured in the previous microscopic analysis, although some relevant differences emerge. In fact, several particles clearly appear as bright spots distributed throughout the varnish layer (Figure 7a,d; P2) together with some air bubbles. The dispersion is clearly visible also when the fragment is observed perpendicularly through a stereomicroscope under visible illumination (Figure 7e). The virtual 3D reconstruction of the volume (Figure 7f) clearly depicts the dispersion of the particles embedded in the coating system.

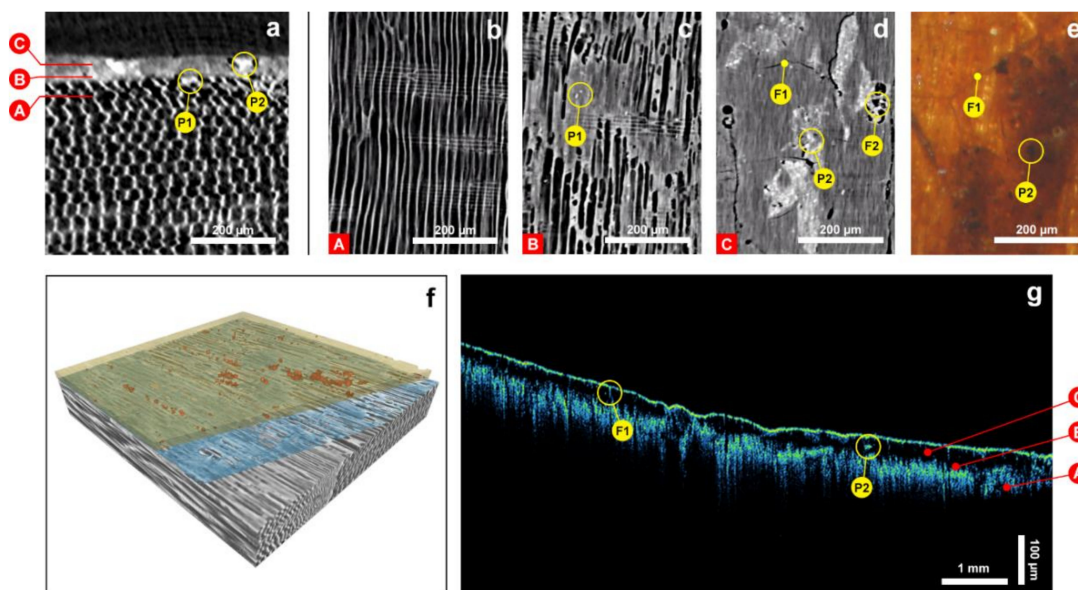


Figure 7. Fragment F21, Lorenzo Guadagnini. (a) Transverse slice from the SR-micro-CT volume with the identified layers; the different kinds of particles embedded in the finishing layers are highlighted as P1 and P2. (b–d) Radial slices from the SR-micro-CT volume showing the finishing layers discussed in the text and reporting the particles P1 and P2 indicated in (a) and identified at different depths. Cracks and air bubbles are indicated as F1 and F2, respectively. (e) Stereomicroscopic image of the surface showing the particles P2, embedded in the finishing layers. (f) Virtual reconstruction based on SR-micro-CT volume. The preparation layer (B in Figure 7a) is colored in blue and the varnish layer C is shown in yellow with particles colored in red. (g) OCT tomogram presented in false-color scale (see Section 2.2 for details). The wood substrate A, the preparation layer, and the varnish layer C are shown. Particles embedded in the varnish and cracks are indicated as P2 and F1, respectively.

The results obtained by OCT (Figure 7g) are consistent with those elaborated with micro-CT: the thickness of the barely detectable preparation layer (B), measures some 12–15 μm and that of the thicker varnish layer (C) varies from approximately 30 μm to about 50 μm . As highlighted in Figure 7g, despite the inorganic nature of P1 particles, they are not detectable in the preparation layer B. Conversely, the bigger grains dispersed in the layer C are visible (Figure 7g; P2), as well as the diffuse cracks formed in this varnish layer (Figure 7g; F1).

4. Conclusions

As the set of samples here considered can represent convincingly—albeit not exhaustively—the variety of situations that can be encountered when coating systems on historical bowed string instruments are considered, the overall results deserve some general comments.

Optical microscopy performed on cross-sections under visible or UV illumination—and scanning electron microscopy as a second step—appears basically as the most efficient way to discriminate the layers. Under the optical microscope with UV illumination, many thin layers may be distinguished according to their different fluorescence, as in the case of fragment F13 [11]. If the number of layers detected by microscopy is set as a benchmark, we can conclude that both the two considered tomographic techniques have mostly reached equal to lower performances. It appears that the more complex is the stratigraphy, the less efficient is the capability of the tomographic techniques to detect differences between the (very thin) layers, as in these cases the thickness of the layers reaches the limits for the spatial resolution of the tomographic setup. Besides this, no clear trend emerges when the two tomographic techniques are compared on their capability of highlighting the number of different layers. If the possibility of local inhomogeneity is considered, we can conclude that the SR-micro-CT and OCT show approximately the same performances for systems up to three levels. With more complex

systems (F13), the higher spatial resolution of SR-micro-CT may enable the better discrimination of some of the layers in comparison to OCT. On the other hand, in two cases (namely in fragments F13 and F20), the SR-micro-CT images failed the detection of a thin preparation layer spread over the wood, which has been instead detected through the OCT tomograms.

Both tomographic techniques have mostly allowed the determination of the thickness of each identified layer. For these values, a large variability is expected, as the layers were spread by a brush, and a comparison among data obtained in different areas is therefore inconclusive.

As for the particles dispersed within the layers, the possibility of obtaining 3D virtual reconstructions from SR-micro-CT volumes, with further post-processing treatment by an image editing software, is helpful to highlight the general features of the coating system. The presence—or the lack—of a preparation layer, the position of the particles in each layer, the presence of a multi/bimodal grain size distribution are valuable information for a preliminary characterization of the coating system, which is particularly relevant as the picture can be obtained by SR-micro-CT without sampling. The OCT tomograms offered, instead, a poorer representation of the particles (due to a worse lateral resolution in comparison to axial one), and possible improvements can be envisaged on this topic in the future, as an example by developing a specific software for the data treatment.

The most beneficial aspect of the tomographic approach in the investigation of such complex layered structures is related to the possibility of obtaining a picture of the undisturbed material. As only micro-samples can normally be obtained, the invasive procedure of the sampling may deform the original structures, leading to erroneous interpretations of the morphology as a result of the manufacturing process. Therefore, the SR-micro-CT 3D virtual representations and the OCT tomograms obtained here represent a further non-invasive in-depth view into the coating systems produced by the four ancient Masters of violin-making.

Author Contributions: Conceptualization, G.F. and M.G.; Data Curation, G.F., T.R., C.I., A.R., M.I. and P.T.; Funding Acquisition, M.M., M.L. and A.L.G.; Investigation, G.F., T.R., C.I., M.A., A.R., G.N.L., F.Z., M.I., P.T. and M.G.; Methodology, F.Z. and P.T.; Supervision, M.M. and M.G.; Validation, G.F., T.R., C.I., A.R., G.N.L., M.I. and P.T.; Visualization, G.F., A.R., M.I. and P.T.; Writing—Original Draft, G.F., T.R., C.I., M.A., M.I., P.T. and M.G.; Writing—Review & Editing, G.F., T.R., C.I., M.A., M.M., M.L., A.R., A.L.G., G.N.L., F.Z., M.I., P.T., and M.G.

Funding: The OCT data were obtained within the Access to Research Infrastructures activity in the H2020 Programme of the EU (IPERION CH Grant Agreement No. 654028). The SR-micro-CT experiments at Elettra were performed within the proposal No. 20170163. The research was financed by the Arvedi Buschini Foundation and by the Università degli Studi di Torino (ricerca locale 2016 and NEXTO project-Progetti di Ateneo 2017).

Acknowledgments: The authors are grateful to the International Violin Making School of Cremona, particularly to M. Alessandro Voltini for providing the fragments of the historical musical instruments. The authors also thank Nicola Sodini for his valuable help in setting up the positioning system at the Synchrotron facility.

Conflicts of Interest: The authors declare no conflict of interest.

References

1. Setragno, F.; Zanoni, M.; Antonacci, F.; Sarti, A.; Malagodi, M.; Rovetta, T.; Invernizzi, C. Feature-based analysis of the impact of ground coat and varnish on violin tone qualities. *Acta Acust. United Acust.* **2017**, *103*, 80–93. [[CrossRef](#)]
2. Jalovec, K. *Beautiful Italian Violins*; P. Hamlyn: London, UK, 1963.
3. Fichera, G.V.; Albano, M.; Fiocco, G.; Invernizzi, C.; Licchelli, M.; Malagodi, M.; Rovetta, T. Innovative monitoring plan for the preventive conservation of historical musical instruments. *Stud. Conserv.* **2017**, *63*, 351–354. [[CrossRef](#)]
4. Invernizzi, C.; Fichera, G.V.; Licchelli, M.; Malagodi, M. A non-invasive stratigraphic study by reflection FT-IR spectroscopy and UV-induced fluorescence technique: The case of historical violins. *Microchem. J.* **2018**, *138*, 273–281. [[CrossRef](#)]

5. Invernizzi, C.; Rovetta, T.; Licchelli, M.; Malagodi, M. Mid and Near-Infrared Reflection Spectral Database of Natural Organic Materials in the Cultural Heritage Field. *Int. J. Anal. Chem.* **2018**. [[CrossRef](#)] [[PubMed](#)]
6. Rovetta, T.; Invernizzi, C.; Licchelli, M.; Cacciatori, F.; Malagodi, M. The elemental composition of Stradivari's musical instruments: New results through non-invasive EDXRF analysis. *X-ray Spectrom.* **2018**, *47*, 159–170. [[CrossRef](#)]
7. Dondi, P.; Lombardi, L.; Invernizzi, C.; Rovetta, T.; Malagodi, M.; Licchelli, M. Automatic analysis of UV induced fluorescence imagery of historical violins. *JOCCH* **2017**, *10*, 1–12. [[CrossRef](#)]
8. Invernizzi, C.; Daveri, A.; Vagnini, M.; Malagodi, M. Non-invasive identification of organic materials in historical stringed musical instruments by reflection infrared spectroscopy: A methodological approach. *Anal. Bioanal. Chem.* **2017**, *409*, 3281–3288. [[CrossRef](#)]
9. Daher, C.; Drieu, L.; Bellot-Gurlet, L.; Percot, A.; Paris, C.; Le Hô, A.-S. Combined approach of FT-Raman, SERS and IR micro-ATR spectroscopies to enlighten ancient technologies of painted and varnished works of art. *J. Raman Spectrosc.* **2014**, *45*, 1207–1214. [[CrossRef](#)]
10. Rovetta, T.; Invernizzi, C.; Fiocco, G.; Albano, M.; Licchelli, M.; Gulmini, M.; Alf, G.; Fabbri, D.; Rombolà, A.G.; Malagodi, M. The case of Antonio Stradivari 1718 ex-San Lorenzo violin: History, restorations and conservation perspectives. *J. Archaeolog. Sci. Rep.* **2019**, *23*, 443–450. [[CrossRef](#)]
11. Fichera, G.V.; Rovetta, T.; Fiocco, G.; Alberti, G.; Invernizzi, C.; Licchelli, M.; Malagodi, M. Elemental analysis as statistical preliminary study of historical musical instruments. *Microchem. J.* **2018**, *137*, 309–317. [[CrossRef](#)]
12. Fiocco, G.; Rovetta, T.; Gulmini, M.; Piccirillo, A.; Licchelli, M.; Malagodi, M. Spectroscopic analysis to characterize finishing treatments of ancient bowed string instruments. *Appl. Spectrosc.* **2017**, *71*, 2477–2487. [[CrossRef](#)] [[PubMed](#)]
13. Echard, J.P.; Lavedrine, B. Review on the Characterisation of ancient stringed musical instruments varnishes and implementation of an analytical strategy. *J. Cult. Heritage* **2008**, *9*, 420–429. [[CrossRef](#)]
14. Barlow, C.Y.; Woodhouse, J. Of old wood and varnish: Peering into the can of worms. *Catgut. Acoust. Soc. J. Ser. II* **1989**, *1*, 2–9.
15. Nagyvary, J.; Guillemette, R.N.; Spiegelman, C.H. Mineral preservatives in the wood of Stradivari and Guarneri. *PLoS ONE* **2009**, *4*, e4245. [[CrossRef](#)] [[PubMed](#)]
16. Echard, J.P.; Bertrand, L.; von Bohlen, A.; Le Ho, A.S.; Paris, C.; Bellot-Gurlet, L.; Soulier, B.; Lattuati-Derieux, A.; Thao, S.; Robinet, L.; et al. The nature of the extraordinary finish of Stradivari's instruments. *Angew. Chem.* **2010**, *49*, 197–201. [[CrossRef](#)] [[PubMed](#)]
17. Tai, B.H. Stradivari's Varnish: A review of scientific findings—Part I. *J. Violin Soc. Am.* **2007**, *21*, 119–144.
18. Fiocco, G.; Rovetta, T.; Gulmini, M.; Piccirillo, A.; Canevari, C.; Licchelli, M.; Malagodi, M. Approaches for detecting madder lake in multi-layered coating systems of historical bowed string instruments. *Coatings* **2018**, *8*, 171. [[CrossRef](#)]
19. Caruso, F.; Chillura Martino, D.F.; Saverwyns, S.; Van Bos, M.; Burgio, L.; Di Stefano, C.; Peschke, G.; Caponetti, E. Micro-analytical identification of the components of varnishes from South Italian historical musical instruments by PLM, ESEM-EDX, microFTIR, GC-MS, and Py-GC-MS. *Microchem. J.* **2014**, *116*, 31–40. [[CrossRef](#)]
20. Tai, B.H. Stradivari's Varnish: A review of scientific findings—Part II. *J. Violin Soc. Am.* **2009**, *22*, 1–31.
21. Echard, J.P. In situ multi-element analyses by energy-dispersive X-ray fluorescence on varnishes of historical violins. *Spectrochim. Acta B* **2004**, *59*, 1663–1667. [[CrossRef](#)]
22. Michelman, J. *Violin Varnish: A Plausible Re-Creation of the Varnish Used by the Italian Violin Makers Between the Years 1550 and 1750, A.D.*, 1st ed.; Joseph Michelman: Cincinnati, OH, USA, 1946; pp. 58–154.
23. Morigi, M.P.; Casali, F.; Bettuzzi, M.; Brancaccio, R.; D'Errico, V. Application of X-ray Computed Tomography to Cultural Heritage diagnostics. *Appl. Phys. A* **2010**, *100*, 653. [[CrossRef](#)]
24. Borman, T.; Stoel, B. Review of the Uses of Computed Tomography for Analyzing Instruments of the Violin Family with a Focus on the Future. *J. Violin Soc. Am. VSA Pap.* **2009**, *22*, 1–12.
25. Latour, G.; Echard, J.P.; Soulier, B.; Emond, I.; Vaiedelich, S.; Elias, M. Structural and optical properties of wood and wood finishes studied using optical coherence tomography: Application to an 18th century Italian violin. *Appl. Opt.* **2009**, *48*, 6485–6491. [[CrossRef](#)] [[PubMed](#)]

26. Sedighi-Gilani, M.; Pflaum, J.; Hartmann, S.; Kaufmann, R.; Baumgartner, M.; Schwarze, F.W.M.R. Relationship of vibro-mechanical properties and microstructure of wood and varnish interface in string instruments. *Appl. Phys. A* **2016**, *122*, 260. [[CrossRef](#)]
27. Lämmlein, S.L.; Mannes, D.; Schwarze, F.W.M.R.; Burgert, I.; Sedighi-Gilani, M. Combined Experimental and Numerical Investigation of Vibro-Mechanical Properties of Varnished Wood for Stringed Instruments. In *Model Validation and Uncertainty Quantification, Volume 3*; Barthorpe, R., Platz, R., Lopez, I., Moaveni, B., Papadimitriou, C., Eds.; Springer: Berlin, Germany, 2017; pp. 81–83.
28. Re, A.; Lo Giudice, A.; Nervo, M.; Buscaglia, P.; Luciani, P.; Borla, M.; Greco, C. The importance of tomography studying wooden artefacts: A comparison with radiography in the case of a coffin lid from Ancient Egypt. *Int. J. Conserv. Sci.* **2016**, *7*, 935–944.
29. Re, A.; Corsi, J.; Demmelbauer, M.; Martini, M.; Mila, G.; Ricci, C. X-ray tomography of a soil block: A useful tool for the restoration of archaeological finds. *Heritage Sci.* **2015**, *3*, 4. [[CrossRef](#)]
30. Re, A.; Albertin, F.; Avataneo, C.; Brancaccio, R.; Corsi, J.; Cotto, G.; De Blasi, S.; Dughera, G.; Durisi, E.; Ferrarese, W.; et al. X-ray tomography of large wooden artworks: The case study of “Doppio corpo” by Pietro Piffetti. *Heritage Sci.* **2014**, *2*, 19. [[CrossRef](#)]
31. Sodini, N.; Dreossi, D.; Chen, R.; Fioravanti, M.; Giordano, A.; Herrestal, P.; Rigon, L.; Zanini, F. Non-invasive microstructural analysis of bowed stringed instruments with synchrotron radiation X-ray microtomography. *J. Cult. Heritage* **2012**, *13*, S44–S49. [[CrossRef](#)]
32. Sodini, N.; Dreossi, D.; Giordano, A.; Kaiser, J.; Zanini, F.; Zikmund, T. Comparison of different experimental approaches in the tomographic analysis of ancient violins. *J. Cult. Heritage* **2017**, *27*, S88–S92. [[CrossRef](#)]
33. Fiocco, G.; Rovetta, T.; Malagodi, M.; Licchelli, M.; Gulmini, M.; Lanzafame, G.; Zanini, F.; Lo Giudice, A.; Re, A. Synchrotron radiation micro-computed tomography for the investigation of finishing treatments in historical bowed string instruments: Issues and perspectives. *Eur. Phys. J. Plus* **2018**, *133*, 525. [[CrossRef](#)]
34. Liang, H.; Cid, M.G.; Cucu, R.G.; Dobre, G.M.; Podoleanu, A.G.; Pedro, J.; Saunders, D. En-face optical coherence tomography—A novel application of non-invasive imaging to art conservation. *Opt. Express* **2005**, *13*, 6133–6144. [[CrossRef](#)] [[PubMed](#)]
35. Targowski, P.; Rouba, B.J.; Wojtkowski, M.; Kowalczyk, A. Application of optical coherence tomography to non-destructive examination of museum objects. *Stud. Conserv.* **2004**, *49*, 107–114. [[CrossRef](#)]
36. Targowski, P.; Iwanicka, M.; Rouba, B.J.; Frosinini, C. OCT for Examination of Artwork. In *Optical Coherence Tomography: Technology and Applications*; Drexler, W., Fujimoto, J., Eds.; Springer: Cham, Switzerland, 2015; pp. 2473–2495.
37. Targowski, P.; Iwanicka, M. Optical Coherence Tomography: Its role in the non-invasive structural examination and conservation of cultural heritage objects—A review. *Appl. Phys. A* **2012**, *106*, 265–277. [[CrossRef](#)]
38. Spotti, G. *Gaetano e Pietro Sgarabotto. Liutai-Violin Makers, (1878–1990)*; Turris: Cremona, Italy, 1991.
39. Cloetens, P.; Pateyron-Salomé, M.; Buffiere, J.Y.; Peix, G.; Baruchel, J.; Peyrin, F.; Schlenker, M. Observation of microstructure and damage in materials by phase sensitive radiography and tomography. *J. Appl. Phys.* **1997**, *81*, 5878–5886. [[CrossRef](#)]
40. Brun, F.; Massimi, L.; Fratini, M.; Dreossi, D.; Billè, F.; Accardo, A.; Pugliese, R.; Cedola, A. SYRMEP Tomo Project: A graphical user interface for customizing CT reconstruction workflows. *Adv. Struct. Chem. Imaging* **2017**, *3*, 1–4. [[CrossRef](#)] [[PubMed](#)]
41. Brun, F.; Accardo, A.; Kourousias, G.; Dreossi, D.; Pugliese, R. Effective implementation of ring artifacts removal filters for synchrotron radiation microtomographic images. In *Proceedings of the International Symposium on Image and Signal Processing and Analysis (ISPA 2013)*, Trieste, Italy, 4–6 September 2013; Ramponi, G., Loncaric, S., Carini, A., Egiazarian, K., Eds.; IEEE: Trieste, Italy, 2013; Volume 17, pp. 672–676.
42. Paganin, D.; Mayo, S.C.; Gureyev, T.E.; Miller, P.R.; Wilkins, S.W. Simultaneous phase and amplitude extraction from a single defocused image of a homogeneous object. *J. Microsc.* **2002**, *206*, 33–40. [[CrossRef](#)] [[PubMed](#)]
43. Herman, G.T. *Image Reconstruction from Projections: The Fundamentals of Computerized Tomography*, 1st ed.; Academic Press: New York, NY, USA, 1980.

44. Iwanicka, M.; Lanterna, G.; Lalli, C.G.; Innocenti, F.; Sylwestrzak, M.; Targowski, P. On the application of optical coherence tomography as a complimentary tool in an analysis of the 13th century Byzantine Bessarion reliquary. *Microchem. J.* **2016**, *125*, 75–84. [[CrossRef](#)]
45. Oct4art—Optical Coherence Tomography for Examination of Work of Art. Available online: <http://www.oct4art.eu/> (accessed on 20 December 2018).



© 2019 by the authors. Licensee MDPI, Basel, Switzerland. This article is an open access article distributed under the terms and conditions of the Creative Commons Attribution (CC BY) license (<http://creativecommons.org/licenses/by/4.0/>).